Journal of Materials Chemistry C

Morphotropic Domain Structure and Phase Components in High-TC Ferroelectric Single Crystals of a Ternary Perovskite Solid Solution

Journal:	*Journal of Materials Chemistry C*
Manuscript ID	TC-ART-03-2018-001198.R1
Article Type:	Paper
Date Submitted by the Author:	16-Jul-2018

Complete List of Authors:	Luo, Zeng; Xi'an Jiaotong University, a. Electronic Materials Research Laboratory, Key Laboratory of the Ministry of Education & International Center for Dielectric Research Zhang, Nan; Xi'an Jiaotong University, a. Electronic Materials Research Laboratory, Key Laboratory of the Ministry of Education & International Center for Dielectric Research Liu, Zenghui; Xi'an Jiaotong University, a. Electronic Materials Research Laboratory, Key Laboratory of the Ministry of Education & International Center for Dielectric Research Zhuang, Jian; Xi'an Jiaotong University, a. Electronic Materials Research Laboratory, Key Laboratory of the Ministry of Education & International Center for Dielectric Research Zhao, Jinyan; Xi'an Jiaotong University, a. Electronic Materials Research Laboratory, Key Laboratory of the Ministry of Education & International Center for Dielectric Research Ye, Z.-G; Simon Fraser University, Department of Chemistry Ren, Wei; Xi'an Jiaotong University,

Journal Name

ARTICLE

Complex Morphotropic Domain Structure and Piezo-/ferroelectric Properties in High-T_C Ferroelectric Single Crystals of a Ternary Perovskite Solid Solution

Received 00th January 20xx,
Accepted 00th January 20xx

DOI: 10.1039/x0xx00000x

www.rsc.org/

Zeng Luo,[a] Nan Zhang, *[a] Zenghui Liu, [a] Jian Zhuang, [a] Jinyan Zhao, [a] Wei Ren [a] and Zuo-Guang Ye *[b,a]

Ferroelectric and piezoelectric materials with a high Curie temperature (T_C) have attracted increasing interest due to the need in applications under extreme conditions. In this work, novel high- T_C ferroelectric single crystals of (0.95-*x*)$BiScO_3$-0.05$Pb(Cd_{1/3}Nb_{2/3})O_3$-*x*$PbTiO_3$ (BS-PCN-*x*PT) ternary solid solution with different compositions have been successfully grown. With increasing PT concentration, a composition-induced structural crossover from a rhombohedral phase, through morphotropic phase boundary (MPB), to a tetragonal phase, is observed. A monoclinic phase (space group *Pm*) is found at the MPB region. The temperature dependences of the dielectric permittivity reveal high Curie-temperatures of 363 °C ~ 452 °C (at 1 MHz). The macroscopic and mesoscopic ferroelastic/ferroelectric domain structures systemically characterized by polarized light microscopy (PLM) and piezoresponse force microscopy (PFM) reveal the existence of monoclinic domains in the crystals with the MPB composition. In monoclinic crystals, the remnant polarization (33.2 μC/cm^2) is weaker than in the rhombohedral phase. All compositions show a high coercive field (around E_C=40 kV/cm). The presence of high T_C and stable poled state signifie that the BS-PCN-*x*PT single crystals are promising candidates for applications such as electromechanical transducers that can be operated in a wide range.

Introduction

Materials with high piezoelectricity and high Curie-temperature (T_C) have been widely needed for various applications, such as underwater sonars, aerospace crafts, combustion engines, etc,[1,2] where they are required to function in severe environments. However, most of the piezoelectrics with large piezoelectric response have a relatively low T_C. For example, $Pb(Zn_{1/3}Nb_{2/3})O_3$–$PbTiO_3$ (PZNT) and $Pb(Mg_{1/3}Nb_{2/3})O_3$–$PbTiO_3$ (PMNT) single crystals have a very high piezoelectric coefficient d_{33} around 2500 pC/N ,[3–7] but a low Curie temperatures around 140-170 °C and an even lower depoling temperatures T_d around 60-120 °C， which limit the temperature range for applications. Therefore, searching for materials with high Curie temperature and decent piezoelectric properties that can be used in extreme environment is an urgent task.

In the search for the novel perovskites with optimized properties, solid solutions with morphotropic phase boundary (MPB) have been considered as the most promising candidates. $PbZr_{1-x}Ti_xO_3$ (PZT) is the first solid solution that was found to have an MPB, in which compositions the material exhibits the highest dielectric and piezoelectric responses. Noheda *et al.* discovered an intermediate monoclinic (*C*m) phase in the MPB region of PZT[8] as a structural bridge between the non-group-subgroup-related rhombohedral (*R*3*m*) and tetragonal (*P*4*mm*) phases. This discovery opened up a series of structural studies on the nature of the MPB,[9–12] including the investigations of local structures which have shed light on the mechanism of the high piezoelectric properties.[13] Although the relationship between the crystal structure and the good properties in the MPB region has not been fully understood, the low-symmetry phase is recognized to play a key role in the appearance of high piezoelectric properties both in terms of intrinsic[14] and extrinsic contributions[15].

On the other hand, due to the concerns about lead toxicity, there have been increasing efforts to develop lead-free or lead-reduced piezoelectrics. One of the lead-reduced solid solution systems that possess an MPB is (1-*x*)$BiScO_3$-*x*$PbTiO_3$ (BS-PT), which shows a high Curie temperature (T_C ~ 450 °C) and good piezoelectric properties.[16] The BS-PT single crystals with different compositions were reported to have a high Curie-temperature of 460 °C (34BS-66PT) and good piezoelectric performance (d_{33} ~ 1150 pC/N) in (43BS-57PT).[17–21] However, scandium oxide is a very expensive compound, which makes BS-PT unsuitable for commercial manufacture and industrial applications. A number of researches were carried out by chemical substitutions on the perovskite B site, like $Bi(Sc_{1-y}Ga_y)O_3$–$PbTiO_3$, $Bi(Sc_{3/4}In_{1/4})O_3$-$PbTiO_3$ and $Bi(Sc_{1-y}Fe_y)O_3$–$PbTiO_3$ systems, some of which exhibited a high Curie temperature (above 430 °C), but at the expense of the

[a] Electronic Materials Research Laboratory, Key Laboratory of the Ministry of Education & International Center for Dielectric Research, Xi'an Jiaotong University, Xi'an 710049, China.
[b] Department of Chemistry and 4D LABS, Simon Fraser University, Burnaby, British Columbia, V5A 1S6, Canada.
*Email - zye@sfu.ca

Electronic Supplementary Information (ESI) available: [details of any supplementary information available should be included here]. See DOI: 10.1039/x0xx00000x

piezoelectric properties which were significantly decreased.[22–24] Some other researchers tried to introduce a third member into the BS-PT binary system to reduce the scandium content. In this way, good piezoelectric properties were achieved, but at the expense of decreasing the Curie temperature.[23,25–33] In addition, (0.95-*x*)$BiScO_3$-0.05$Pb(Cd_{1/3}Nb_{2/3})O_3$-*x*$PbTiO_3$ (BS-PCN-*x*PT) polycrystalline ceramics were reported.[34] $Pb(Cd_{1/3}Nb_{2/3})O_3$ is a relaxor ferroelectric material belonging to the complex perovskite family. Previous work[35] illustrates that $Pb(Cd_{1/3}Nb_{2/3})O_3$ has two temperatures of dielectric anomaly or maximum (T_m): the low temperature one at ~ -33 °C and the high temperature at about 387 °C. 0.86$PbTiO_3$-0.14$Pb(Cd_{1/3}Nb_{2/3})O_3$, added some suitably modified additives like WO_3, MnO_2 and NiO, shows good electrical properties and its Curie temperature is over 450 °C[36]. It was also found that the BS-PCN-*x*PT ceramics with compositions near the MPB (*x*=0.60) showed the best piezoelectric performance, with a Curie temperature of 403 °C and a piezoelectric coefficient (d_{33}) of 505 pC/N. The properties of the BS-PCN-PT ceramics are comparable with those of the BS-PT ceramics and other ternary systems but not as good as the BS-PT single crystals, even though the electric performance of the BS-PCN-PT ceramics was greatly enhanced in the MPB compositions.[34] Therefore, to achieve high T_C and high piezoelectricity and to understand the domain structures and structural features of this solid solution system, single crystals are needed.

In this work, we have grown single crystals of the ternary BS-PCN-*x*PT system for the first time, and characterized the electric properties and the domain structures, which shed light on their relevant physical mechanisms between phase structures and electric properties.

Experiments

Single crystals of BS-PCN-*x*PT were grown using a traditional method, namely "top-cooled solution growth" (TCSG) method. The raw powders of PbO (99.9%), Bi_2O_3 (99.9%), TiO_2 (98%), Sc_2O_3 (99.99%), CdO (99%), and Nb_2O_5 (99.5%) were selected as the starting materials and were weighed according to the stoichiometry of the select compositions. The nominal compositions for different batches were chosen to maintain the content of PCN unchanged at 5%, the same as the ceramics reported in Ref. 35. The percentage of PT ranged from 50% to 60%. The starting materials of BS-PCN-*x*PT were then mixed with the flux of (60wt%PbO + 40wt%Bi_2O_3) at an optimized ratio of flux: solute = 6:1 in weight. The mixture was thoroughly ground for 0.5 h and then placed into a 50 ml Pt crucible. A small amount of B_2O_3 was added into the mixture to stabilize the growth of the crystals and to improve their quality. The loaded Pt crucible was put into a larger alumina crucible, which was then placed inside the crystal growth furnaces. The top-cooling was achieved by a platinum wire via its great thermal conduction which triggered nucleation around it. The following thermal program was used: heating up to 1150 °C, soaking for 24 h, and cooling at 0.2 °C/h to 850 °C. The crystals were leached out from the solidified flux in a 30 % HNO_3 solution.

All the grown crystals exhibit a rectangular shape with a size of 2~4 mm and a good quality. The samples from different batches for electric measurements were cut parallel to the naturally grown {001} § face. Crystals of the highest quality were finely polished down to 80~100 μm thick for optical studies. Because the domain structure is sensitive to stresses, the samples were annealed without external electric field at 500 °C for 1 h to release the stresses involved in the cutting and polishing processes.

X-ray diffraction experiments on powder samples obtained from crashed small crystals were performed on a PANalytical Empyrean diffractometer with Cu $K\alpha$1 X-ray tube to analyse the structures of the grown crystals. Single crystal diffraction measurements were carried out on a bulk crystal by using a PANalytical X'Pert MRD diffractometer (40 kV, 30 mA). Polarized light microscopy (PLM) experiments were performed with an Olympus BX-51 polarizing microscope equipped with a Linkam (THMS600E) heating stage to study the domain structures and phase transitions of the grown crystals. The domain structures were also imaged by piezoresponse force microscopy (PFM) with a modified commercial atomic force microscopic system in piezoresponse mode (AFM, Dimension ICON, NanoScope V, Bruker). All the samples for electrical characterization were painted with silver paste on both parallel sides as electrodes. The dielectric properties were measured by an E4981A Precision LCR meter (Agilent, Hewlett-Packard, USA) and a home-made temperature chamber in the range of room temperature to 550 °C with a heating rate of 2 °C/min, which was controlled by a EUROTHERM 3204 PID temperature controller. The polarization-electric field P(*E*) hysteresis loops were measured by the Sawyer-Tower technique using a Radiant RT-66 standardized ferroelectric testing system at room temperature.

Crystal Structure

The XRD patterns of the BS-PCN-*x*PT single crystals with different PT contents are displayed in Figure 1(a). The single {002} peak is found to start splitting when the PT content *x* increases, which indicates a possible phase transition from the rhombohedral to the tetragonal phase. Because of the preferred orientations existing in the powder samples obtained from the crushed crystals, it is difficult to extract crystal structures from the Rietveld refinement[37] which relies on an accurate measurement of the peak shapes and intensities[38]. Therefore, the XRD results were fitted by Pawley refinement method[39] using the TOPAS Academic[40] software to further explore the structural change with composition. The diffraction patterns in the {002}-reflection range (2-Theta = 44° - 46.5°) are presented in Figure 1(b), in which the experimental data are shown by the black dots, while the fitting results are displayed by the red curve. Different structural models have been tried to fit the experimental data. A model with the coexistence of the *P*4*mm* and *R*3*m* phases is found to fit well with the diffraction pattern of Batch #1 crystals. In contrast, neither a single-phase model nor a combination of *P4mm* and *R3m* phases could fit the Batch #2 and #3 crystals diffraction pattern. Therefore, the

structural models consisting a mixture of (*P4mm* + *R3m* + *Pm*) phases and (*P4mm* + *Pm*) phases are used to fit the Batches #2 and #3 data, respectively. The mixture models leading to satisfactory refinement results are shown with blue tics for the *P4mm* phase, green tics for the *R3m* and pink tics for the *Pm* phase, respectively. The fitting results clearly show a gradual transition from the BS-rich rhombohedral phase to the PT-rich tetragonal phase. Therefore, the structure in the MPB region seems to be quite complex with the presence of a monoclinic phase that coexists with the *P*4*mm* and/or *R*3*m* phases.

Dielectric Properties

Figure 2 shows the variations of the dielectric constant and loss tangent as a function of temperature measured at 10 kHz, 100 kHz, and 1 MHz. The phase transition temperatures are indicated by the dielectric peaks at 1 MHz that vary from 362.5 °C to 452 °C when the nominal PT content increases from 0.50 to 0.60. The crystals exhibit suppressed and broader dielectric peaks at lower PT concentrations. As the PT content increases, dielectric peaks become sharpened, suggesting increased ferroelectricity (similar behaviour was observed in the BS-PCN-PT ceramics [34]). Moreover, the loss tangent is lower than 0.4 up to 300 °C, which suggests that the crystals are good dielectric materials suitable for high-temperature applications.

Domain structure and phase symmetry

The mesoscopic ferroelectric and ferroelastic domain structures of the grown BS-PCN-*x*PT crystals are investigated using polarized light microscopy and piezoresponse force microscopy. The principles of optical crystallography are applied to the analysis of the domain structures and phase symmetry. [41–44]

In PLM, the extinction directions of different domains can be identified by changing the positions of the single crystal plates relative to the mutually perpendicular crossed polarizer and analyser. Figure 3(a) and (b) shows the optical axes of the indicatrix along <111> in the rhombohedral phase and along <001> in the tetragonal phase, respectively, which correspond to the spontaneous polarization directions. Therefore, when observed along <001>, a {001} platelet will exhibit domains with extinction angles at 45° to the [100] direction in the rhombohedral (R) phase and 0° or 90° in the tetragonal (T) phase, as shown in Figure 3(d)-(e). Figure 3(c) shows the orientations of spontaneous polarizations (P_S) in the monoclinic M_C phase. There are three main sets of P_S directions for the M_C domains, near the [100], [010], and [001] directions, respectively. Each kind of domain sets has four subvariants due to the distortion of the crystal lattice, as shown in Fig. 3(c). According to Vanderbilt and Cohen[45], the monoclinic M_C (space group *Pm*) structure has {100} mirror plane in which the A/B cations are displaced along [0uv]. Bokov and Ye discussed the extinction law for the M_C phase[43] and pointed out that one of the indicatrix section axes should be perpendicular to the (100) mirror plane and the other two sections may be oriented within the mirror plane at any angles [Figure 3(f)]. As a result, it is possible to observe non-complete extinction areas on the crystal with the M_C symmetry, as the domains with different sets of extinction position may overlap with each other along the direction of observation.

The domain structure of a {001} platelet of a Batch #1 crystal with crossed polarizers at 0° and 45° to the <100> direction are presented in Figure 4(a) and (b). A major part of the sample is at extinction with crossed polarizers at 45° to the <100> direction, indicating a rhombohedral symmetry at room temperature. A small part at the top of the platelet shows tetragonal behaviour (with an extinction angle equal to 90°). Upon heating, the birefringence of the rhombohedral part of Batch #1 platelet becomes zero when the temperature reaches about 350 °C. In contrast, the tetragonal region does not show any phase transition until 446 °C. The difference in phase transition temperatures can be explained by the composition segregation which leads to rhombohedral and tetragonal phases coexisting in the same piece of crystal. This observation is in good agreement with the above-mentioned XRD refinement and dielectric measurements results of Batch #1 crystals.

The BS-PCN-PT single crystal from Batch #3 exhibits large domain areas with extinction oriented parallel to the <100> directions, as shown in Figure 4(c)-(d). Domain walls along the <110> directions formed by domains with mutually perpendicular polarization directions are also observed in some regions of crystal platelet in Fig. 4(d). Those domains belong to the *a* domains[45] in a tetragonal crystal with polarization lying in the {001} plane of the platelet. Combined with X-ray diffraction patterns, this domain structure indicates a tetragonal *P*4*mm* symmetry in the crystals of Batch #3. In addition, small regions with diffraction fringes and no complete extinction are found in Figure 4(c). They are the possible results of strains existing near the ferroelastic domain boundaries.

The PLM images of a (001) crystal from Batch #2 of the MPB composition [Figure 5(a) and (b)] show fine domains with a higher domain wall density compared to the rhombohedral and tetragonal crystals. Two kinds of domain arrangements are observed with different extinction behaviours, as highlighted by the rectangles in Figure 5(b), which are labelled Part 1 and Part 2. The extinction angle of Part 2 is 90°, consistent with a tetragonal or monoclinic M_C symmetry. In contrast, a large area marked by a dashed white rectangle in Figure 5(a), including Part 1, does not show complete extinction at 90°. In fact, no complete extinction can be observed at any angles. This is believed to arise from the domains overlapping with each other. A ω-2θ reciprocal space mapping image obtained from single-crystal diffraction experiment [Fig. 5(c)] shows two reflections at different 2θ values corresponding to the {111} reflection family, which cannot be attributed to a tetragonal phase. The above optical and X-ray results indicate that mostly probably this crystal has the monoclinic M_C structure. This is in good agreement with the previous reports on the existence of lower symmetry phases in BS-PT from X-ray / neutron powder diffraction experiments[21,46].

In comparison to PLM, piezoresponse force microscopy (PFM) measurement is able to achieve relatively high spatial

resolution in a non-destructive way.[47] In the piezoresponse force microscopy experiment, the ferroelectric polar domains on a mesoscopic scale with different polarizations can be distinguished based on the different piezoelectric displacements in the directions normal or parallel to the sample surface scanned by the PFM tip.[48] As long as there is a vertical component of polarization in a {100} crystal platelet, piezoresponse signal can be obtained to form the out-of-plane (OOP) phase image consisting of bright and dark regions. However, for the in-plane (IP) imaging, the tip of PFM is only sensitive to the deformation along the direction which is perpendicular to the scanning direction. Sometimes, piezoresponse phase images are clearly observed by PFM, which is not a physical representation but an artefact of PFM scanning. This can be explained by the notion of crosstalk between OPP signal and IP signal.[49] In this part, the small signal responding to an external AC field with no pressure and no heating was collected to reveal the static local domain structures. The crystals of BS-PCN-PT for PFM experiments are well polished by using aluminium lapping film and mounted onto a piece of silicon with silver paint. The PFM experimental setup in this paper was schematically presented in Fig. 6.

Figure 7 shows the OOP and IP amplitude images and phase images obtained by PFM for the {001} crystals from Batch #1, Batch #2 and Batch #3 with different domain sizes, about 0.6 μm for Batch #1, 1.0 μm for Batch #2 and 1.5 μm for Batch #3. McGilly[49] mentioned that the domain width was dramatically larger using PFM than using transmission electron microscopy (TEM), which suggests differences in the surface energy densities caused by different boundary conditions in the two modes of imaging. Unlike TEM, PLM and PFM imaging were both performed in air. The domain size of BS-PCN-PT crystals was observed to be in accordance with those in PLM images, which demonstrates no influence of boundary conditions.

The Batch #1 crystal [Figure 7(a)] shows fingerprint-like patterns with a 180° phase angle in both the out-of-plane and in-plane images, indicating the presence of 180° ferroelectric domains. For the Batch #2 crystal, given that the polarization of the *Pm* (M_C) phase lies on the {100} mirror plane, a vertical component and a horizontal component of P_S can be detected by PFM at the same time on a {001} platelet as long as the mirror plane is perpendicular to the scanning direction. In the PFM images, shown in Figure 7(b), the 180° ferroelectric domains are observed in both the OOP and IP phase images with a ferroelastic domain boundary which is non-45° to the [100] direction, as marked with the blue line. The 180° ferroelectric domains are also present, embedded within each ferroelastic domain as the fingerprint-like pattern. For a (001)-cut single crystal with tetragonal structure, signals can be observed in either the OOP or IP phase images but not simultaneously: in a typical tetragonal *c*-domain, the PFM response is only found in the out-of-plane direction while in an *a*-domain, the PFM signal only arises from the in-plane direction. This is exactly what we have found in the crystal from Batch #3 [Figure 7(c)], i.e. the IP image shows no PFM signal.

More detailed investigations have been performed on a Batch #2 crystal for its interesting domain structures. Figure 8 (a and b) show the domain patterns in part 2 (Figure 5). Broad stripe-like ferroelastic domains with orientation close to a [110] direction (49.5° to the [100] direction) in Figure 8 are consistent with those in Figure 5. The domain widths range from 9 to 30 μm. The blue lines in Figure 8 (a and b) mark two stripe domains including a wide one named A and a narrow one named B. Ferroelectric domains embedded inside the ferroelastic domains were found to have a width around 1.0 μm. Similar domain arrangements in PMN-PT single crystal with M_C symmetry were also reported by Bai *et al*[50]. Similar to what is found in Fig. 7(b), signals are observed in both OPP and IP phase images. To figure out whether it is caused by the crosstalk between OPP and IP, the differences of the piezo-responses before and after rotating the crystal by 90° are discussed. Before rotation, 180° ferroelectric domains are found in both the OPP and IP phase images, and the domain patterns almost match with each other. This indicates that a three-dimensional polarization results in the IP and OOP components simultaneously in these two phase images. After rotation, both the OOP amplitude and phase images show almost the same signals with the strength unchanged. However, changes are observed in the IP piezoresponse amplitude images. The signal strength in the A area becomes weaker after rotation. In contrast, the signal strength in B becomes stronger. This relative changes in IP amplitude images which cannot be attributed to a rhombohedral or tetragonal phase. Since there will be no changes in IP phase due to the positions of polarizations. Combine other results mentioned above, an explanation may come from the monoclinic phase. Further studies on the specific polarization orientation in the domains of the M_C phase are underway.

Ferroelectric Properties

Polarization-electric field (P-E) hysteresis loops of the BS-PCN-*x*PT crystals were displayed at room temperature, as shown in Figure 9, which demonstrate the ferroelectric nature of the grown crystals. It can be seen that saturation of polarization is achieved under an electric field of 65 kV/cm at 1 Hz. Note that the P-E loops ($E_{C+} \neq E_{C-}$) appear to be asymmetric for all three crystals, indicating the existence of internal bias fields in the crystals. The largest remnant polarization is found to be *Pr*=38.7 μC/cm² with a coercive electric field E_C = 43.05 kV/cm for Batch #1 crystal in the rhombohedral phase. Batch #2 crystal with the MPB composition and Batch #3 crystal show lower remnant polarization values of 33.2 μC/cm² and 27.3 μC/cm², respectively. The average coercive electric fields in Batch #2 and Batch #3, calculated by $(E_{C+} + E_{C-})/2$, are 37.9 kV/cm and 39.2 kV/cm, respectively. It should be noted that the coercive electric fields for all compositions are much higher than that of the PZNT and PMNT crystals (2 - 3 kV/cm) and almost twice that of the BS-PT system (~ 20 kV/cm) near the MPB region, which indicates a stable poled state in these crystals which are suitable for potential applications at high fields.

Conclusions

The single crystals of a new ternary solid solution system of $BiScO_3$-$Pb(Cd_{1/3}Nb_{2/3})O_3$-$PbTiO_3$ have been successfully grown with compositions across the morphotropic phase boundary for the first time. The grown crystals exhibit complex crystal structures and electric properties. The ferroelastic domains of the BS-PCN-PT crystals imaged by polarized light microscopy reveal complex structures characteristic of the different phase symmetries, and in particular confirm the presence of the monoclinic M_C phase when combined with single crystal reciprocal space mapping. The ferroelectric domains are observed in all the crystals by piezoresponse force microscopy. Interestingly, only the crystals in MPB are found to display a variety of ferroelastic domains with the fingerprint like ferroelectric domains embedded in them. Different in-plane amplitude for these crystals are evidenced directly by analysing rotation behaviours under PFM, which supports the monoclinic model even further. Large remnant polarizations and high coercive electric fields are found in three types of crystals, indicating that the BS-PCN-PT crystals have an excellent poled state. These data demonstrated that BS-PCN-PT crystals are promising candidates for high temperature and high field applications.

Acknowledgements

This work was supported by the National Natural Science Foundation of China (NSFC, Grants No. 61604123), "the Fundamental Research Funds for the Central Universities" of China and the “111 project” of China. ZGY's primary affiliation is Simon Fraser University (SFU). The work at SFU was supported by the U.S. Office of Naval Research (ONR, Grants No. N00014-12-1-1045 and N00014-16-1-6301) and the Natural Sciences and Engineering Research Council of Canada (NSERC, Grant No. 203773).

Notes and references

‡ Footnotes relating to the main text should appear here. These might include comments relevant to but not central to the matter under discussion, limited experimental and spectral data, and crystallographic data.

§ Here and throughout the paper we use pseudocubic cell setting for the indexing of lattice directions, Bragg reflections and Miller indices for lattice planes.

1 N. Setter, *Piezoelectric materials in devices: extended reviews on current and emerging piezoelectric materials, technology, and applications*, Ceramics Laboratory, EPFL Swiss Federal Institute of Technology, 2002.

2 Z.-G. Ye, *Handbook of dielectric, piezoelectric and ferroelectric materials Synthesis, properties and applications*, Woodhead Publishing Limited, 2008.

3 X. Zhao, J. Wang, K.-H. Chew, H. L.-W. Chan, C.-L. Choy, Z. Yin and H. Luo, *Mater. Lett.*, 2004, **58**, 2053–2056.

4 K. K. Rajan and L. C. Lim, *Appl. Phys. Lett.*, 2003, **83**, 5277–5279.

5 S. Zhang, L. Lebrun, D.-Y. Jeong, C. A. Randall, Q. Zhang and T. R. Shrout, *J. Appl. Phys.*, 2003, **93**, 9257–9262.

6 S. Zhang, J. Luo, W. Hackenberger, N. P. Sherlock, R. J. Meyer and T. R. Shrout, *J. Appl. Phys.*, 2009, **105**, 104506.

7 D. Viehland, J. Powers, L. E. Cross and J. F. Li, *Appl. Phys. Lett.*, 2001, **78**, 3508–3510.

8 B. Noheda, D. E. Cox, G. Shirane, J. A. Gonzalo, L. E. Cross and S.-E. Park, *Appl. Phys. Lett.*, 1999, **74**, 2059–2061.

9 J. Frantti, S. Ivanov, S. Eriksson, H. Rundlöf, V. Lantto, J. Lappalainen and M. Kakihana, *Phys. Rev. B*, 2002, **66**, 641081–6410815.

10 D. Phelan, X. Long, Y. Xie, Z.-G. Ye, A. M. Glazer, H. Yokota, P. A. Thomas and P. M. Gehring, *Phys. Rev. Lett.*, 2010, **105**, 207601.

11 N. Zhang, H. Yokota, A. M. Glazer and P. A. Thomas, *Acta Crystallogr. Sect. B Struct. Sci.*, 2011, **67**, 386–398.

12 S. Gorfman, D. S. Keeble, A. M. Glazer, X. Long, Y. Xie, Z.-G. Ye, S. Collins and P. A. Thomas, *Phys. Rev. B*, 2011, **84**, 020102.

13 N. Zhang, H. Yokota, A. M. Glazer, Z. Ren, D. A. Keen, D. S. Keeble, P. A. Thomas and Z.-G. Ye, *Nat. Commun.*, 2014, **5**, 5231.

14 H. Fu and R. E. Cohen, *Nature*, 2000, **403**, 281.

15 J. L. Jones, M. Hoffman, J. E. Daniels and A. J. Studer, *Appl. Phys. Lett.*, 2006, **89**, 092901.

16 R. E. Eitel, C. A. Randall, T. R. Shrout, P. W. Rehrig, W. Hackenberger and S.-E. Park, *Jpn. J. Appl. Phys.*, 2001, **40**, 5999–6002.

17 S. Zhang, L. Lebrun, S. Rhee, R. E. Eitel, C. A. Randall and T. R. Shrout, *J. Cryst. Growth*, 2002, **236**, 210–216.

18 S. Zhang, C. A. Randall and T. R. Shrout, *Appl. Phys. Lett.*, 2003, **83**, 3150–3152.

19 S. Zhang, C. A. Randall and T. R. Shrout, *Jpn. J. Appl. Phys.*, 2003, **42**, L1152–L1154.

20 S. Zhang, C. A. Randall and T. R. Shrout, *Solid State Commun.*, 2004, **131**, 41–45.

21 S. Zhang, C. A. Randall and T. R. Shrout, *Jpn. J. Appl. Phys.*, 2004, **43**, 6199–6203.

22 I. Sterianou, D. C. Sinclair, I. M. Reaney, T. P. Comyn and a. J. Bell, *J. Appl. Phys.*, 2009, **106**, 084107.

23 Z. Hu, J. Chen, M. Li, X. Li, G. Liu and S. Dong, *J. Appl. Phys.*, 2011, **110**, 064102.

24 E. D. Politova, G. M. Kaleva, a V Mosunov and a H. Segalla, *Phys. Scr.*, 2014, **89**, 044007.

25 Y. Chen, J. Zhu, D. Xiao, B. Qin and Y. Jiang, *J. Alloys Compd.*, 2009, **470**, 420–423.

26 C. J. Stringer, N. J. Donnelly, T. R. Shrout, C. A. Randall, E. F. Alberta and W. S. Hackenberger, *J. Am. Ceram. Soc.*, 2008, **91**, 1781–1787.

27 T.-H. Song, R. E. Eitel, T. R. Shrout, C. A. Randall and W. Hackenberger, *Jpn. J. Appl. Phys.*, 2003, **42**, 5181–5184.

28 Z. Yao, H. Liu, H. Hao and M. Cao, *J. Appl. Phys.*, 2011, **109**, 014105.

29 M. V. Talanov, A. A. Bush, K. E. Kamentsev, V. P. Sirotinkin and A. G. Segalla, *J. Am. Ceram. Soc.*, 2018, **101**, 683–693.

30 S. Zhang, Y. Yu, J. Wu, X. Gao, C. Huang and S. Dong, *J. Alloys Compd.*, 2018, **731**, 1140–1145.

31 D. Wang, Z. Jiang, B. Yang, S. Zhang, M. Zhang, F. Guo and W. Cao, *Jpn. J. Appl. Phys.*, 2013, **52**, 101101.

32 T. Y. Ansell, D. P. Cann, E. Sapper and J. Rödel, *J. Am. Ceram. Soc.*, 2014, **98**, 455–463.
33 B. Kowalski, A. Sayir and A. Sehirlioglu, *J. Mater. Sci.*, 2016, **51**, 6761–6769.
34 T.-L. Zhao, J. Chen, C.-M. Wang, Y. Yu and S. Dong, *J. Appl. Phys.*, 2013, **114**, 027014.
35 W. Bąk, C. Kajtoch, K. Mroczka and K. Wójcik, *Arch. Mater. Sci. Eng.*, 2008, **33**, 75–78.
36 J. Shenglin, W. Xiaozheng and Z. Xuli, *Ferroelectrics*, 1997, **197**, 155–159.
37 H. M. Rietveld, *J. Appl. Crystallogr.*, 1969, **2**, 65–71.
38 L. B. McCusker, R. B. Von Dreele, D. E. Cox, D. Louër and P. Scardi, *J. Appl. Crystallogr.*, 1999, **32**, 36–50.
39 G. S. Pawley, *J. Appl. Crystallogr.*, 1981, **14**, 357–361.
40 A. A. Coelho, *J. Appl. Crystallogr.*, 2005, **38**, 455–461.
41 K. Aizu, *Phys. Rev. B*, 1970, **2**, 754–772.
42 Z.-G. Ye, B. Noheda, M. Dong, D. Cox and G. Shirane, *Phys. Rev. B*, 2001, **64**, 184114.
43 A. A. Bokov, X. Long and Z.-G. Ye, *Phys. Rev. B*, 2010, **81**, 172103.
44 Z.-G. Ye and M. Dong, *J. Appl. Phys.*, 2000, **87**, 2312–2319.
45 D. Vanderbilt and M. H. Cohen, *Phys. Rev. B*, 2001, **63**, 094108.
46 K. Datta, S. Gorfman and P. A. Thomas, *Appl. Phys. Lett.*, 2009, **95**, 251901.
47 V. V Shvartsman, B. Dkhil and A. L. Kholkin, *Annu. Rev. Mater. Res.*, 2013, **43**, 423–449.
48 A. P. C. Harnagea M. Alexe, and D. Hesse, *Integr. Ferroelectr. 38 667-673*, 2001, **4587**, 113–124.
49 L. McGilly, D. Byrne, C. Harnagea, A. Schilling and J. M. Gregg, *J. Mater. Sci.*, 2009, **44**, 5197–5204.
50 F. Bai, J. Li and D. Viehland, *Appl. Phys. Lett.*, 2004, **85**, 2313–2315.

Table and Figures

Table 1 Nominal composition and growth results of the BS-PCN-PT single crystals obtained from different batches

Batch No.	Nominal composition	Crystal size
1	0.45BS-0.05PCN-0.50PT	2~4 mm
2	0.40BS-0.05PCN-0.55PT	2~3 mm
3	0.35BS-0.05PCN-0.60PT	2~3 mm

Figure caption

Figure 1. (a) XRD patterns of the BS-PCN-xPT crystals. (b) Refinement results of the {002} reflection at room temperature (2-Theta = 43.75° - 46.5°). The black dots represent the measured data. The red curve is the calculated result. Individual phases are also shown in tics with different colours: blue - tetragonal, green - rhombohedral and pink -monoclinic.

Figure 2. Temperature dependences of (a) the dielectric constant (ε'), and (b) the loss tangent (tan δ) of the three batches of crystals.

Figure 3. Schematic presentations of the domain orientations in three crystal symmetries. (a) orientations of the spontaneous polarization (P_S) in a rhombohedral phase; (b) orientations of P_S and optical indicatrix in a tetragonal phase; (c) P_S variants of a monoclinic M_C phase; (d-f) possible extinction positions of the resulting domains with the possible optical indicatrix sections in a (001) crystal plate. In (e), the circle means that some domains are always in extinction.

Figure 4. Domain structures of Batch #1 and Batch #3 {001} crystal platelets observed by PLM with crossed polarizers parallel [(a) and (c)], and at 45° [(b) and (d)], to the <100> direction, respectively.

Figure 5. Domain structure of a {001} platelet from Batch #2 observed by PLM with crossed polarizers parallel (a), and at 45° (b), to the $<100>_{cub}$ direction, respectively. (c) Single crystal XRD ω-2θ images of a BS-PCN-PT crystal (Batch #2), for the {111} reflection.

Figure 6. Schematic diagram of PFM setup

Figure 7. PFM images of the single crystal of (a) Batch #1, (b) Batch #2 and (c) Batch #3 (imaging was performed using a tip voltage of 6 V, and frequency of 34-54 kHz): (1) Out-of-plane piezoresponse amplitude images, (2) Out-of-plane piezoresponse phase images, (3) In-plane piezoresponse amplitude images, and (4) In-plane piezoresponse phase images.

Figure 8. PFM images of a single crystal of Batch #2: (a) Original position and (b) After a 90o counter clockwise rotation (80 μm×80 μm) (OOP=Out-of-plane, IP=In-plane). Crystal structural models with mirror planes perpendicular to [010] (c) and [100] (d). (e) and (f) The in-plane projections of the P_S of the two crystal structures in (c) and (d) viewed along the c-direction before and after rotation.

Figure 9. Ferroelectric properties of the BS-PCN-xPT crystals at room temperature at 1Hz

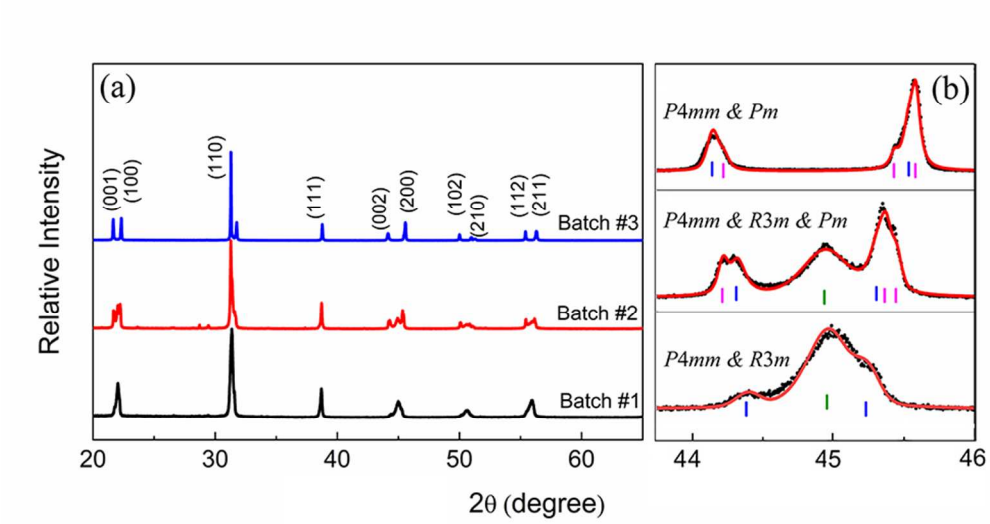

Figure 1 (a) XRD patterns of the BS-PCN-xPT crystals. (b) Refinement results of the {002} reflection at room temperature (2-Theta = 43.75° - 46.5°). The black dots represent the measured data. The red curve is the calculated result. Individual phases are also shown in tics with different colours: blue - tetragonal, green - rhombohedral and pink - monoclinic

82x43mm (300 x 300 DPI)

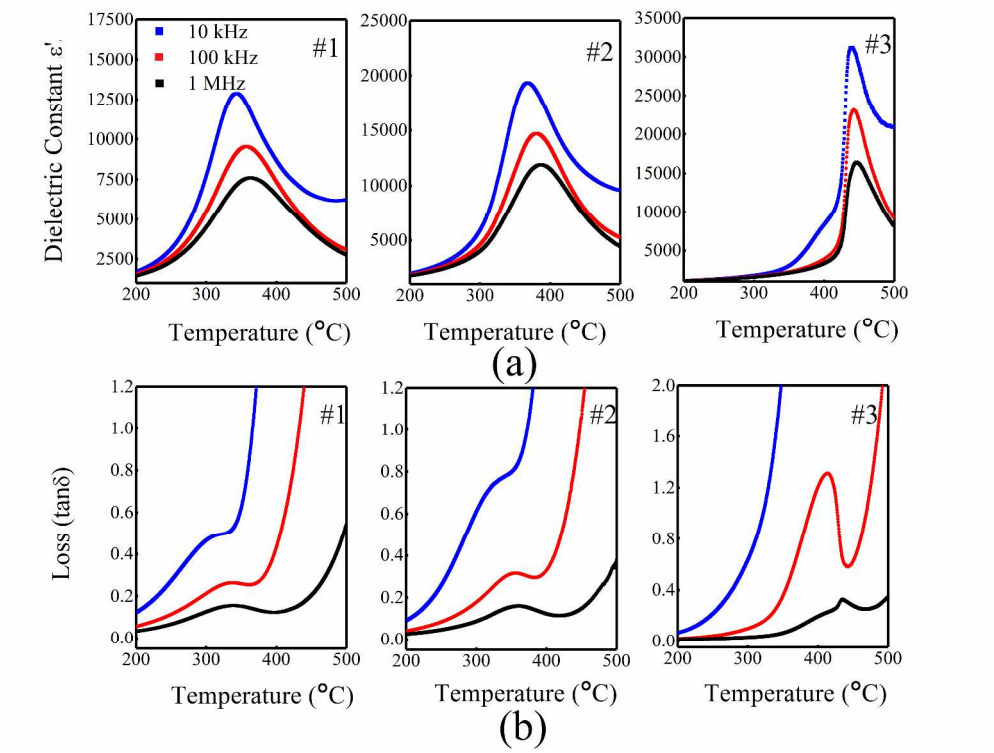

Figure 2 Temperature dependences of (a) the dielectric constant (ε'), and (b) the loss tangent (tan δ) of the three batches of crystals.

508x381mm (300 x 300 DPI)

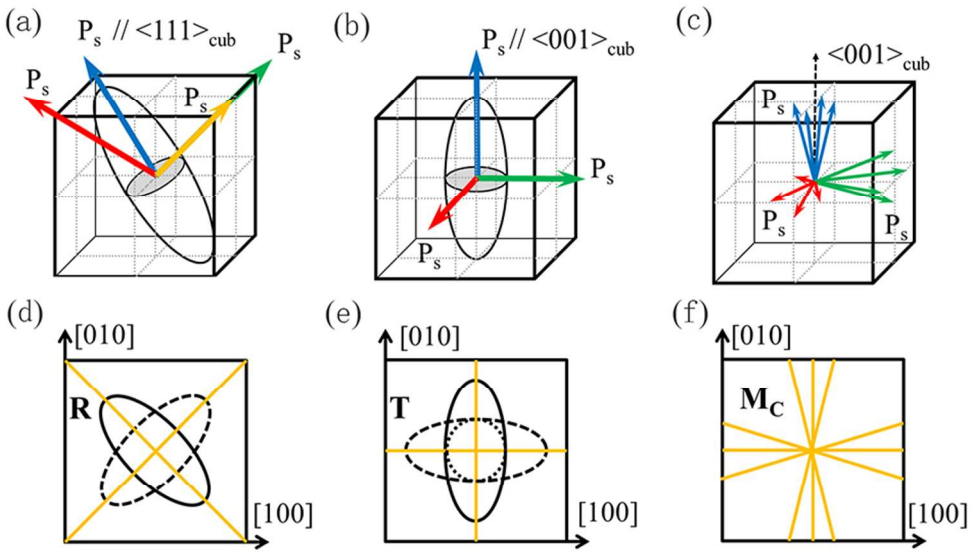

Figure 3 Schematic presentations of the domain orientations in three crystal symmetries. (a) orientations of the spontaneous polarization (P_S) in a rhombohedral phase; (b) orientations of P_S and optical indicatrix in a tetragonal phase; (c) P_S variants of a monoclinic MC phase; (d-f) possible extinction positions of the resulting domains with the possible optical indicatrix sections in a (001) crystal plate. In (e), the circle means that some domains are always in extinction.

82x47mm (300 x 300 DPI)

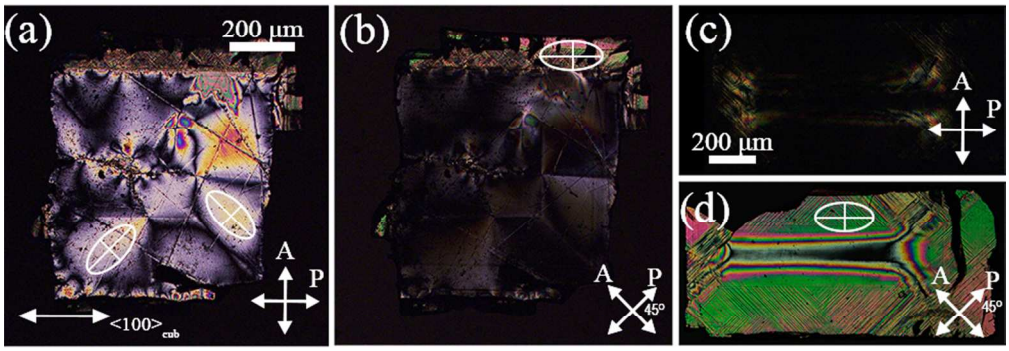

Figure 4 Domain structures of Batch #1 and Batch #3 {001} crystal platelets observed by PLM with crossed polarizers parallel [(a) and (c)], and at 45° [(b) and (d)], to the <100> direction, respectively.

82x38mm (300 x 300 DPI)

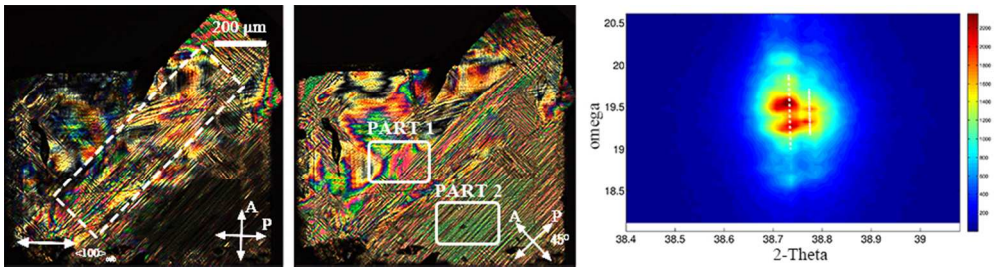

Figure 5 Domain structure of a {001} platelet from Batch #2 observed by PLM with crossed polarizers parallel (a), and at 45° (b), to the <100>cub direction, respectively. (c) Single crystal XRD ω-2θ images of a BS-PCN-PT crystal (Batch #2), for the {111} reflection.

82x21mm (300 x 300 DPI)

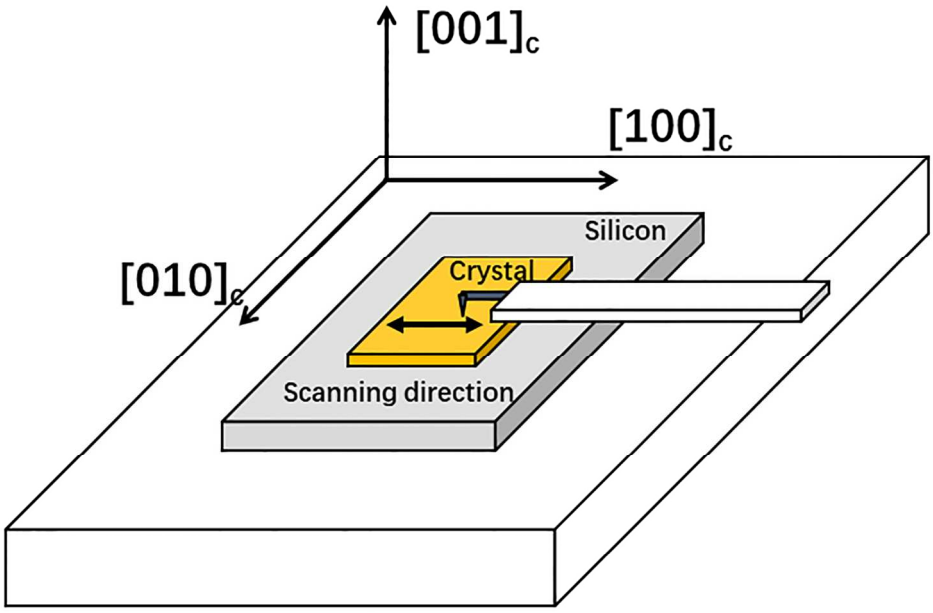

Figure 6 Schematic diagram of PFM setup.

181x125mm (300 x 300 DPI)

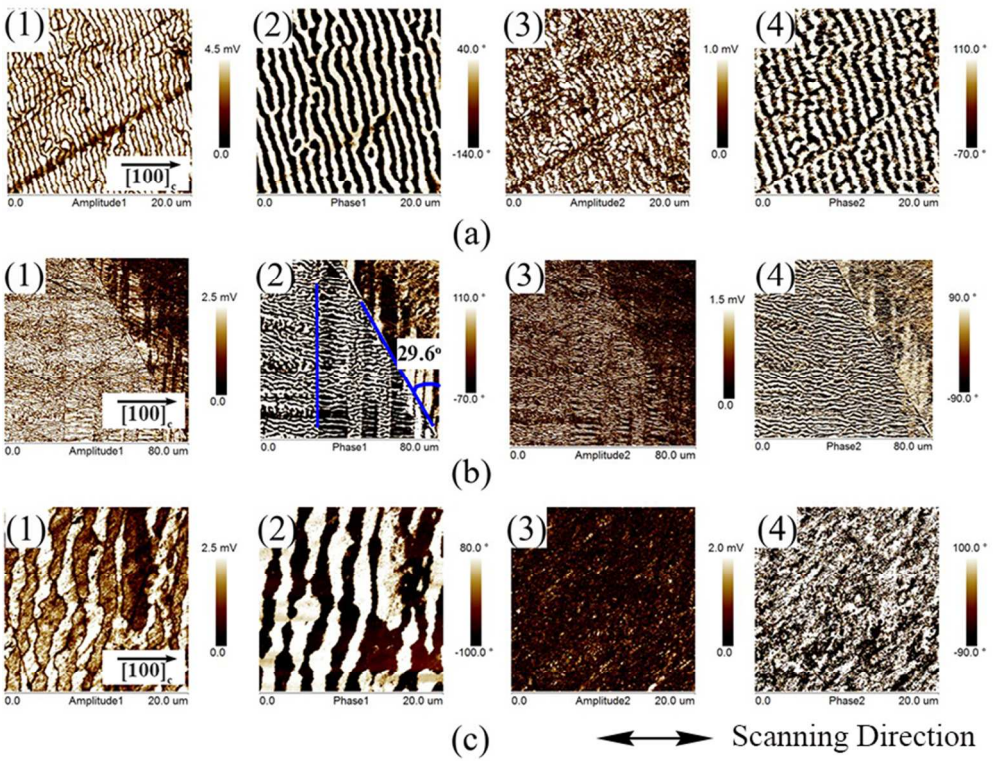

Figure 7 PFM images of the single crystal of (a) Batch #1, (b) Batch #2 and (c) Batch #3 (imaging was performed using a tip voltage of 6 V, and frequency of 34-54 kHz): (1) Out-of-plane piezoresponse amplitude images, (2) Out-of-plane piezoresponse phase images, (3) In-plane piezoresponse amplitude images, and (4) In-plane piezoresponse phase images.

83x65mm (280 x 280 DPI)

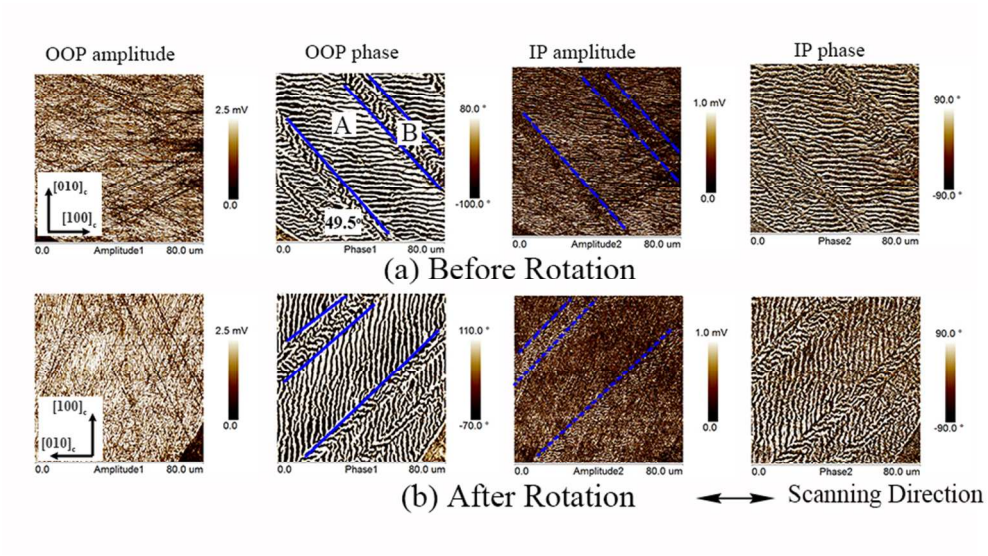

Figure 8 PFM images of a single crystal of Batch #2: (a) Original position and (b) After a 90° counter clockwise rotation (80 μm×80 μm) (OOP=Out-of-plane, IP=In-plane). Crystal structural models with mirror planes perpendicular to [010] (c) and [100] (d). (e) and (f) The in-plane projections of the P_S of the two crystal structures in (c) and (d) viewed along the c-direction before and after rotation.

82x45mm (300 x 300 DPI)

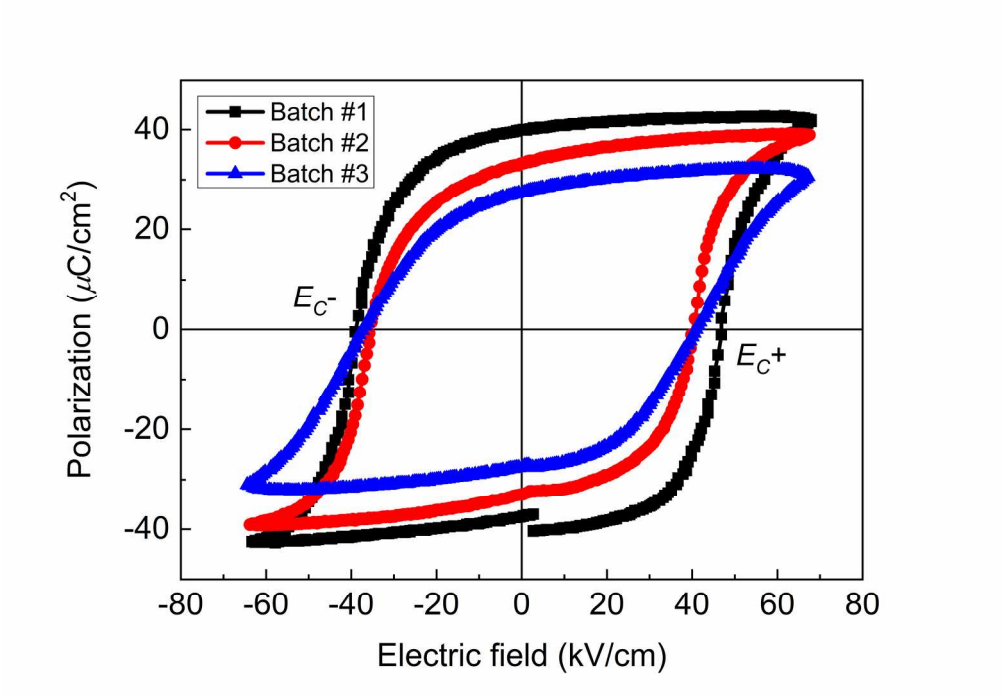

Figure 9 Ferroelectric properties of the BS-PCN-xPT crystals at room temperature at 1Hz

199x139mm (300 x 300 DPI)

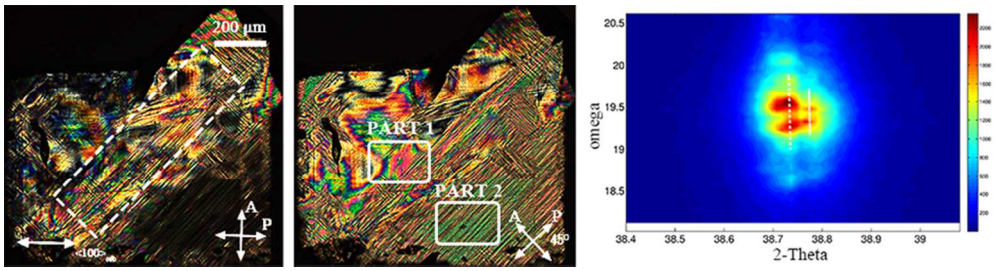

80x20mm (300 x 300 DPI)